Lattice-Boltzmann model for interacting amphiphilic fluids

Maziar Nekovee and Peter V. Coveney

Centre for Computational Science, Department of Chemistry, Queen Mary, University of London, Mile End Road,
London E1 4NS, United Kingdom

Hudong Chen

Exa Corporation, 450 Bedford Street, Lexington, Massachusetts 02173

Bruce M. Boghosian

Center for Computational Science, Boston University, 3 Cummington Street, Boston, Massachusetts 02215
(Received 29 May 2000)

We develop our recently proposed lattice-Boltzmann method for the nonequilibrium dynamics of amphiphilic fluids [H. Chen, B. M. Boghosian, P. V. Coveney, and M. Nekovee, Proc. R. Soc. London, Ser. A **456**, 2043 (2000)]. Our method maintains an orientational degree of freedom for the amphiphilic species and models fluid interactions at a microscopic level by introducing self-consistent mean-field forces between the particles into the lattice-Boltzmann dynamics, in a way that is consistent with kinetic theory. We present the results of extensive simulations in two dimensions which demonstrate the ability of our model to capture the correct phenomenology of binary and ternary amphiphilic fluids.

PACS number(s): 82.70.−y, 47.20.Hw, 64.75.+g

I. INTRODUCTION

The lattice-Boltzmann (LB) method is a mesoscopic approach to the study of the dynamics of fluids, intermediate between macroscopic models, based on Navier-Stokes equations, and microscopic approaches, based on molecular dynamics (MD) simulations. In this method, time, velocity, and space are all discretized and a single-particle distribution function is utilized to describe the time evolution of an ensemble of molecules having a discrete set of possible velocities [1,2]. The computationally demanding tracking of individual molecules is thus avoided and at the same time the ensemble-averaged distribution function retains much of the microscopic information. Macroscopic or hydrodynamic effects naturally emerge from mesoscale lattice-Boltzmann dynamics, provided that the LB equation possesses the correct and necessary conservation laws and symmetries [1]. Historically, the lattice-Boltzmann model was first derived from its predecessor—the lattice-gas automata (LGA) [3–6]—but it has been shown recently that the model can also be derived from kinetic theory by discretization of the Boltzmann equation in velocity, space, and time [7,8].

An important and promising area of application of the lattice-Boltzmann method is for modeling the dynamics of multicomponent fluids. There is in particular much fundamental and technological interest in modeling amphiphilic systems; i.e., fluids comprising one or two immiscible phases (such as oil and water) and an amphiphilic species (surfactant). The addition of surfactant to a binary immiscible fluid can result in complex structures on a mesoscopic length scale, including lamellar, micelles and microemulsion phases [9,10]. The nonequilibrium dynamics and hydrodynamics of these systems are difficult to simulate using a continuum approach based on Navier-Stokes equations. One major difficulty these methods face is the existence of complicated interfaces between fluid components which can undergo topological changes; another is that it is far from clear how to formulate a hydrodynamic description of these fluids. Microscopic approaches, based on molecular dynamics, are able to deal with amphiphilic fluids, but they are still computationally too demanding to investigate large-time dynamics (times scales accessible to MD are typically of the order of nanoseconds [11] whereas important time scales in such complex fluids vary between $10^{-11}-10^4$ s) and the extended spatial structures involved in many problems of interest.

The formation of fluid interfaces is a consequence of interaction between the molecules of the fluids [12], and the LB models for multicomponent fluids come in two varieties, depending on the way interactions between fluid components are incorporated. In the free-energy approach [12–15] the starting point is an *ansatz* for the free-energy functional of the complex interacting fluid and the approach to equilibrium is assumed to be governed by a Ginzburg-Landau or Cahn-Hillard equation or some suitable generalization thereof. A LB collision operator is then constructed that gives rise to the desired evolution equation in the hydrodynamic limit. The most attractive feature of this model is that the equilibrium state is fixed *a priori* by the choice of free-energy functional. This guarantees thermodynamic consistency at equilibrium but limits the description of nonequilibrium dynamics. For example, the one-component free energy model is not Galilean invariant [16]. Furthermore, the method relies on the ability to postulate a suitable form for the free energy, which might not be always available. An alternative approach, which is closer in spirit to kinetic theory, is to add interactions between fluid components by introducing intermolecular forces between fluid particles [17,24]. Very recently we proposed such a lattice-Boltzmann model for amphiphilic fluids [25] which is based on introducing the dynamics and interactions of amphiphilic molecules into the multicomponent lattice-Boltzmann scheme of Shan and Chen [17]. In the resulting ternary vector model, which was inspired by the lattice-gas automata (LGA) formalism of Boghosian Coveney and Emerton [26],

amphiphilic species possess both translational and orientational degrees of freedom, a feature which is crucial for capturing much of the abovedescribed phenomenology of amphiphilic systems.

The principal aim of the present paper is to further develop and explore this model and to assess and establish its general validity for modeling the dynamics of amphiphilic systems. In Sec. II we give a detailed description of the model and show that with slight modification, the mean-field treatment of intermolecular interactions in the model [17,25] can be made consistent with the mean-field kinetic theory of interacting fluids, based on a set of coupled Boltzmann equations. In Sec. III we use this modified model to simulate the nonequilibrium dynamics of binary immiscible and binary and ternary amphiphilic fluids in two dimensions. These simulations demonstrate that the model exhibits the correct dynamical behavior in the case of critical quenches of binary fluids and it is capable of describing in a consistent way the phenomenology of various experimentally observed self-assembling structures, such as lamellae, droplet and sponge microemulsion phases, the arrest of separation of immiscible oil-water phases when enough surfactant is present in the system, and the formation of the lamellar phases in binary water-surfactant systems. Finally, in Sec. V we draw some conclusions from this work and discuss the prospects of future developments of the model.

II. LATTICE-BOLTZMANN MODEL FOR INTERACTING FLUID MIXTURES

The lattice-Boltzmann scheme for a fluid mixture having S components is defined in terms of the distribution functions $f_i^\sigma(\mathbf{x},t)$ belonging to the particles of component σ of the fluid mixture (e.g., σ = water or oil in a binary system). In the BGK approximation [19] of the collision operator these equations are [2,7]

$$f_i^\sigma(\mathbf{x}+\mathbf{c}_i\Delta t,t+\Delta t)-f_i^\sigma(\mathbf{x},t)=-\frac{f_i^\sigma-f_i^{\sigma(\mathrm{eq})}}{\lambda_\sigma}\Delta t, \quad (1)$$

where $\mathbf{c}_i$ ($i=0,1,\ldots,M$) are a set of discrete velocity vectors on a regular lattice, $\mathbf{x}$ is a point on the underlying spatial grid, $f_i^{\sigma(\mathrm{eq})}$ is a local equilibrium distribution function, λ_σ is the relaxation time for component σ, and Δt is the time step.

The number density n^σ and the mean velocity $\mathbf{u}^\sigma$ of component σ are given by

$$n^\sigma(\mathbf{x},t)=\sum_i f_i^\sigma, \quad (2)$$

$$\rho^\sigma(\mathbf{x},t)u^\sigma(\mathbf{x},t)=m^\sigma\sum_i \mathbf{c}_i f_i^\sigma, \quad (3)$$

with $\rho^\sigma=m^\sigma n^\sigma$ the density and m^σ the mass of species σ.

The equilibrium distribution function should be chosen in such a way that the BGK collision operator $\Omega_i^\sigma=-(f_i^\sigma-f_i^{\sigma(\mathrm{eq})})/\lambda_\sigma$ locally conserves the mass of each species σ

$$\sum_i \Omega_i^\sigma=0. \quad (4)$$

We also require that the momentum of all components together should be conserved locally

$$\sum_\sigma m_\sigma\sum_i \mathbf{c}_i\Omega_i^\sigma=0. \quad (5)$$

A common choice which satisfies the above constraints is [20,21]

$$f_i^{\sigma(\mathrm{eq})}=\omega_i n^\sigma\left[1+\frac{1}{c_s^2}\mathbf{c}_i\cdot\tilde{\mathbf{u}}+\frac{1}{2c_s^4}(\mathbf{c}_i\cdot\tilde{\mathbf{u}})^2-\frac{1}{2c_s^2}\tilde{u}^2\right], \quad (6)$$

where ω_i is a weight factor and c_s is the speed of sound, both of which are determined entirely by the choice of lattice. For example, in the so-called D3Q19 lattice [21] (19 velocity vectors in three dimensions) $c_s=1/\sqrt{3}$ and $\omega_i=1/3$, 1/18, and 1/36 for $e_i=0$, $e_i=1$, and $e_i=2$, respectively.

The requirement that the total velocity of all components together should be conserved at each lattice point results in the following form for the common velocity $\tilde{\mathbf{u}}$

$$\tilde{\mathbf{u}}=\frac{\displaystyle\sum_\sigma \frac{\rho^\sigma\mathbf{u}^\sigma}{\tau_\sigma}}{\displaystyle\sum_\sigma \frac{\rho^\sigma}{\tau_\sigma}}, \quad (7)$$

where we have introduced the dimensionless relaxation time $\tau_\sigma=\lambda_\sigma/\Delta t$.

In the limit of small Mach numbers, i.e., $\tilde{u}/c_s\ll 1$, where the right-hand side of Eq. (6) is positive, the above choice of $f_i^{\sigma(\mathrm{eq})}$ results in Navier-Stokes hydrodynamics, where each fluid component σ has kinematic viscosity $\nu_\sigma=(\tau_\sigma-1/2)c_s^2$ [20].

A. Mean-field treatment of interactions

In order to describe immiscibility effects, some form of repulsive interaction between fluid components must be introduced into the LB equations. In the Shan-Chen scheme [17], coupling between fluid components is achieved by including intermolecular interactions in the model. These interactions are modeled as a self-consistently generated mean-field force. Allowing only homogeneous isotropic interactions between nearest-neighbors, the mean-field force $\mathbf{F}^\sigma$ acting on particles of component σ is given by

$$\mathbf{F}^\sigma(\mathbf{x},t)=-\psi^\sigma(\mathbf{x},t)\sum_\sigma\sum_{\mathbf{x}'} g_{\sigma\bar\sigma}\psi^{\bar\sigma}(\mathbf{x}',t)(\mathbf{x}'-\mathbf{x}), \quad (8)$$

where $\psi^\sigma=\psi^\sigma[\rho^\sigma(\mathbf{x},t)]$ is the so-called effective mass, which can have a general form for modeling various types of fluids (in the present study we have taken $\psi^\sigma=\rho^\sigma$) and $g_{\sigma\bar\sigma}$ is a force coupling constant, whose magnitude controls the strength of the interaction between component σ and $\bar\sigma$ and whose sign determines whether this interaction is repulsive ($g_{\sigma\bar\sigma}>0$) or attractive ($g_{\sigma\bar\sigma}<0$). Shan and Chen incorporated the above force term in the LB dynamics by adding an increment [17]

$$\delta\mathbf{u}^\sigma = \frac{\mathbf{F}^\sigma}{\rho^\sigma}\Delta t \tag{9}$$

to the velocity $\widetilde{\mathbf{u}}$ which enters the equilibrium distribution function (6) in the BGK collision operator.

With the choice $\psi^\sigma = \rho^\sigma$ the above treatment of intermolecular interactions is consistent with kinetic theories of interacting fluids, in which non-local interactions are described by including a self-consistently generated mean-field force term in the Boltzmann equation while local interactions are treated as true collisions. Indeed, kinetic equations of this type have been successfully applied to describe gas-gas separation into two phases [22] and, more recently, spinodal decomposition in binary fluids [27]. However, the way the mean-field force enters the Shan-Chen model is not entirely consistent with the Boltzmann equation in the presence of a force [28,29]. The explicit expression for the force term in the Shan-Chen model can be obtained by substituting $\widetilde{\mathbf{u}} + \delta\mathbf{u}$ into the equilibrium distribution function. This yields

$$f_i^\sigma(\mathbf{x}+\mathbf{c}_i\Delta t, t+\Delta t) - f_i^\sigma(\mathbf{x},t)$$
$$= -\frac{f_i^\sigma - f_i^{\sigma_i(\mathrm{eq})}}{\tau_\sigma} + \omega_i n^\sigma \left[\frac{\mathbf{c}_i - \widetilde{\mathbf{u}}}{c_s^2} + \frac{(\mathbf{c}_i \cdot \widetilde{\mathbf{u}})}{c_s^4}\mathbf{c}_i \right] \mathbf{a}_\sigma \Delta t$$
$$-\frac{1}{2}\omega_i n^\sigma \left[\frac{a_\sigma^2}{c_s^2} - \frac{(\mathbf{c}_i \cdot \mathbf{a}_\sigma)^2}{c_s^4} \right] \tau_\sigma \Delta t^2, \tag{10}$$

where $\mathbf{a}_\sigma = \mathbf{F}^\sigma/\rho^\sigma$ is force per unit mass. As was shown by Luo [28] and by Martys $et\ al.$ [29], by omitting the second order term in $\mathbf{a}_\sigma$ the above equation can be made consistent with a systematic derivation of the lattice-Boltzmann model in the presence of the force $\mathbf{a}_\sigma$, as obtained from discretization of the corresponding Boltzmann equation, in the low Mach-number regime. In our scheme we omit this non-linear term when calculating the effect of the self-consistently generated mean-field force, so that the resulting lattice-Boltzmann scheme is consistent with the underlying Boltzmann equation in the presence of a force. Our final lattice-Boltzmann equation is then given by

$$f_i^\sigma(\mathbf{x}+\mathbf{c}_i\Delta t, t+\Delta t) - f_i^\sigma(\mathbf{x},t)$$
$$= -\frac{f_i^\sigma - f_i^{\sigma_i(\mathrm{eq})}}{\tau_\sigma} + \omega_i n^\sigma \left[\frac{\mathbf{c}_i - \widetilde{\mathbf{u}}}{c_s^2} + \frac{(\mathbf{c}_i \cdot \widetilde{\mathbf{u}})}{c_s^4}\mathbf{c}_i \right] \mathbf{a}_\sigma \Delta t. \tag{11}$$

In the case of a single-component interacting fluid, rewriting the force term in terms of distribution functions n_i^σ leads to the following lattice-Boltzmann equation:

$$f_i^\sigma(\mathbf{x}+\mathbf{c}_i\Delta t, t+\Delta t) - f_i^\sigma(\mathbf{x},t) = -\frac{f_i^\sigma - f_i^{\sigma_i(\mathrm{eq})}}{\tau_\sigma} + \sum_j \Lambda_{ij}^{\sigma\sigma} f_j^\sigma, \tag{12}$$

where $\Lambda_{ij}^{\sigma\sigma}$ is given by

$$\Lambda_{ij}^{\sigma\sigma} = \omega_i \left[\frac{1}{c_s^2}(\mathbf{c}_i - \mathbf{c}_j) + \frac{\mathbf{c}_i \cdot \mathbf{c}_j}{c_s^4}\mathbf{c}_i \right] \mathbf{a}_\sigma \Delta t. \tag{13}$$

Thus the net effect of the force term is to introduce off-diagonal matrix elements in the BGK collision operators. These matrix elements describe transitions from state $\mathbf{c}_i$ to state $\mathbf{c}_j$, and $vice\ versa$, due to the drift of particles under the influence of the force during the time Δt. In the case of a fluid mixture the BGK collision operator couples different fluid components even in the absence of the mean-field force, through the common velocity $\widetilde{\mathbf{u}}$ which enters $f_i^{\sigma(\mathrm{eq})}$. The mean-field force introduces an additional non-local coupling between fluid particles and in this case Eq. (11) can be rewritten as

$$f_i^\sigma(\mathbf{x}+\mathbf{c}_i\Delta t, t+\Delta t) - f_i^\sigma(\mathbf{x},t)$$
$$= -\frac{f_i^\sigma - f_i^{\sigma_i(\mathrm{eq})}}{\tau_\sigma} + \sum_{\bar\sigma} \sum_j \Lambda_{ij}^{\sigma\bar\sigma} f_j^{\bar\sigma}, \tag{14}$$

where $\Lambda_{ij}^{\sigma\bar\sigma}$ are matrix elements of the cross-collision operator

$$\Lambda_{ij}^{\sigma\bar\sigma} = \omega_i \left[\frac{1}{c_s^2}(\delta_{\sigma\bar\sigma}\mathbf{c}_i - \alpha_{\sigma\bar\sigma}\mathbf{c}_j) + \alpha_{\sigma,\bar\sigma}\frac{\mathbf{c}_i \cdot \mathbf{c_j}}{c_s^4}\mathbf{c}_i \right] \mathbf{a}_\sigma \Delta t \tag{15}$$

with

$$\alpha_{\sigma\bar\sigma} = \frac{n^\sigma}{n^{\bar\sigma}} \times \frac{\dfrac{\rho^{\bar\sigma}}{\tau_{\bar\sigma}}}{\displaystyle\sum_{\bar\sigma}\frac{\rho^{\bar\sigma}}{\tau_{\bar\sigma}}}. \tag{16}$$

The above treatment of intermolecular interactions does not take into account strong repulsive interactions between molecules at short distance which prevent them to overlay (the excluded volume effect [23]). This effect is important in calculating transport coefficients of dense gases and fluids [23] but we do not expect it to significantly alter the dynamics of microemulsions, which is the main focus of our present work. The excluded volume effect can be introduced in the model by adding Enskog corrections to the BGK collision operator [24].

B. Modeling surfactant dynamics and interactions

A surfactant (or amphiphilic) molecule usually possesses two different fragments, each having an affinity for one of the two immiscible components. In the case of a prototype mixture of immiscible fluids such as oil and water, a typical surfactant molecule would be an amphiphile that has a hydrophilic head preferring to be in contact with water molecules, and a hydrophobic tail preferring to be surrounded by oil. Under equilibrium conditions the surfactants are predominantly adsorbed at the oil-water interface, hence effectively screening the two-body repulsive interaction between immiscible species. In our scheme [25] these essential characteristics of amphiphilic molecules are modeled by introducing a separate amphiphilic species into the Shan-Chen

model which possesses both translational and rotational degrees of freedom. This is achieved by modeling these species as idealized point dipoles. Consequently, the interaction of the amphiphilic molecules with each other and with nonamphiphilic molecules (such as oil and water) depends not only on their relative distance but also on their dipolar orientation [26]. Furthermore, a full description of the dynamics of amphiphilic molecules requires a description of the propagation of each single-particle distribution function as well as the time evolution of their dipole vectors. Making the physically reasonable assumption that the dipole moment carried by amphiphilic molecules is independent of their velocity, an average dipole vector $\mathbf{d}(\mathbf{x},t)$ is introduced at each site $\mathbf{x}$ representing the orientation of any amphiphile present there. The propagation of the amphiphilic molecules is then described in our scheme by a set of BGK-like equations, one for the distribution function f_i^s and one for the relaxation of the average dipole vector $\mathbf{d}(\mathbf{x},t)$ to its local equilibrium orientation [25]:

$$f_i^s(\mathbf{x}+\mathbf{c}_i\Delta t,t+\Delta t)-f_i^s(\mathbf{x},t)$$
$$=-\frac{f_i^s-f_i^{s(\text{eq})}}{\tau_s}+\sum_\sigma\sum_j\Lambda_{ij}^{\sigma s}f_j^\sigma+\sum_j\Lambda_{ij}^{ss}f_j^s,$$
(17)

$$\mathbf{d}(\mathbf{x},t+\Delta t)=\overline{\mathbf{d}}(\mathbf{x},t)-\frac{1}{\tau_d}[\overline{\mathbf{d}}(\mathbf{x},t)-\mathbf{d}^{\text{eq}}(\mathbf{x},t)].\quad(18)$$

In the above equations $f_i^s(\mathbf{x},t)$ is the distribution function of surfactant molecules and τ_s and τ_d are dimensionless relaxation times representing the rates of relaxation of $f_i^s(\mathbf{x},t)$ and $\mathbf{d}(\mathbf{x},t)$ to their local equilibrium distributions $f_i^{s(\text{eq})}$ and $\mathbf{d}^{eq}(\mathbf{x},t)$, respectively. The collision operators $\Lambda_{ij}^{\sigma s}$ and Λ_{ij}^{ss} have the same form as Eq. (15) and describe the effect of the total mean-field force experienced by surfactant particles due to their interactions with nonamphiphilic particles and with other amphiphilic particles. We shall specify these forces shortly. Finally, $\overline{\mathbf{d}}(\mathbf{x},t)$ is obtained from the following equation of motion:

$$n^s(\mathbf{x},t)\overline{\mathbf{d}}(\mathbf{x},t)=\sum_i f_i^s(\mathbf{x}-\mathbf{c}_i\Delta t)\mathbf{d}(\mathbf{x}-\mathbf{c}_i\Delta t,t).\quad(19)$$

The equilibrium distribution function $f_i^{s(\text{eq})}$ is chosen to have the same form as Eq. (6) and, in analogy with the Weiss molecular field theory of magnetism [30], the equilibrium distribution $\mathbf{d}^{\text{eq}}(\mathbf{x},t)$ is obtained self-consistently from the Boltzmann distribution as

$$\mathbf{d}^{\text{eq}}(\mathbf{x},t)=d_0\frac{\int e^{-\beta U}\hat{\mathbf{v}}d\Omega}{\int e^{-\beta U}d\Omega},\quad(20)$$

where $d\Omega$ is an element of solid angle, $\hat{\mathbf{v}}$ is a unit vector, and U is the potential energy of a dipole in the mean field generated by dipolar amphiphiles and nonamphiphilic molecules

$$U=-\hat{\mathbf{v}}\cdot(\mathbf{h}_s+\mathbf{h}_c).\quad(21)$$

In Eq. (21) $\mathbf{h}_s$ and $\mathbf{h}_c$ are the mean fields resulting from dipole-dipole interactions and the interaction between surfactant dipoles and nonamphiphilic molecules, respectively. In Eq. (20) both d_0 and the inverse temperature β, are independent parameters. Performing the integral yields for the equilibrium distribution

$$\mathbf{d}^{\text{eq}}=d_0\left[\coth(\beta h)-\frac{1}{\beta h}\right]\hat{\mathbf{h}}\quad(22)$$

in 3D and

$$\mathbf{d}^{\text{eq}}=d_0\left[\frac{I_1(\beta h)}{I_0(\beta h)}\right]\hat{\mathbf{h}}\quad(23)$$

in 2D, where h is the magnitude of $\mathbf{h}=\mathbf{h}_s+\mathbf{h}_c$, and I_0 and I_1 are the zero and the first order modified Bessel functions [31], respectively.

The mean-field generated by water and oil molecules is given by

$$\mathbf{h}^c(\mathbf{x},t)=\sum_\sigma e_\sigma\sum_i n^\sigma(\mathbf{x}+\mathbf{c}_i\Delta t,t)\mathbf{c}_i,\quad(24)$$

where e_σ is the "charge" for various molecular components (which may take its values from the set $\{-1,0,1\}$). In the present simulations we take $e=1$ for water molecules and $e=-1$ for oil molecules. Similarly, the mean-field generated by other surfactant molecules is given by

$$\mathbf{h}^s(\mathbf{x},t)=\sum_i\left[\sum_{j\neq 0}n_i^s(\mathbf{x}+\mathbf{c}_j\Delta t,t)\boldsymbol{\theta}_j\cdot\mathbf{d}_i(\mathbf{x}+\mathbf{c}_j\Delta t,t)\right.$$
$$\left.+n_i^s(\mathbf{x},t)\mathbf{d}_i(\mathbf{x},t)\right],\quad(25)$$

where

$$\boldsymbol{\theta}_j=\mathbf{I}-D\frac{\mathbf{c}_j\mathbf{c}_j}{c_j^2}$$

is the traceless second-rank tensor and D is dimension of the lattice.

Finally, we specify the form of interaction between amphiphilic molecules with water and oil particles and between amphiphilic molecules themselves. These are obtained from Eq. (8) by treating each amphiphilic molecule as a pair of water and oil molecules displaced by a distance $\mathbf{d}(\mathbf{x},t)$ from each other and performing a Taylor expansion in $\mathbf{d}$ in the resulting expression for the total force [25]. Assuming that the dipole head and tail have equal and opposite charges $e=\pm 1$ and with only nearest-neighbor interactions considered, the additional forces are given by

$$\mathbf{F}^{\sigma,s}(\mathbf{x},t)=-2\psi^\sigma(\mathbf{x},t)g_{\sigma s}\sum_{i\neq 0}\mathbf{d}(\mathbf{x}+\mathbf{c}_i\Delta t)$$

$$\times\left(\mathbf{I}-\frac{\mathbf{c}_i\mathbf{c}_i}{c_i^2}D\right)\psi^s(\mathbf{x}+\mathbf{c}_i\Delta t,t),\quad(26)$$

$$\mathbf{F}^{s,c}(\mathbf{x},t) = 2\,\psi^s(\mathbf{x},t)\mathbf{d}(\mathbf{x},t)$$

$$\times \sum_\sigma \, g_{\sigma s}\sum_{i\neq 0}\left(\mathbf{I}-\frac{\mathbf{c}_i\mathbf{c}_i}{c_i^2}D\right)\psi^\sigma(\mathbf{x}+\mathbf{c}_i,t), \tag{27}$$

and

$$\mathbf{F}^{s,s}(\mathbf{x},t) = -\frac{4D}{c^2}g_{ss}\psi^s(\mathbf{x})\sum_i\left\{\mathbf{d}(\mathbf{x}+\mathbf{c}_i\Delta t,t)\mathbf{d}(\mathbf{x},t):\right.$$

$$\left[\mathbf{I}-\frac{\mathbf{c}_i\mathbf{c}_i}{c_i^2}D\right]\mathbf{c}_i + [\mathbf{d}(\mathbf{x}+\mathbf{c}_i\Delta t,t)\mathbf{d}(\mathbf{x},t)$$

$$\left.+\mathbf{d}(\mathbf{x},t)\mathbf{d}(\mathbf{x}+\mathbf{c}_i\Delta t,t)]\cdot\mathbf{c}_i\right\}\psi^s(\mathbf{x}+\mathbf{c}_i+\Delta t,t). \tag{28}$$

In the above equations $\mathbf{F}^{\sigma,s}$ is the force acting on nonamphiphilic particles σ (water and oil) due to amphiphile dipoles, $\mathbf{F}^{s,c}$ is the force acting on amphiphilic molecules due to all nonamphiphilic particles, and $\mathbf{F}^{s,s}$ is the force among amphiphilic molecules themselves. The coupling constants $g_{\sigma s}$ and g_{ss} determine, respectively, the strength of interaction between water and oil molecules and surfactant molecules, and among surfactant molecules themselves. The coupling coefficient g_{ss} should be chosen negative if we wish to model attraction between two amphiphile heads or tails, and repulsion between a head and a tail.

III. SIMULATIONS

As mentioned earlier the principal aim of the present work is to assess the ability of our model to reproduce the basic properties of self-assembling amphiphilic fluids. For this reason we choose not to explore the entire parameter space of the model in the present study but rather find through a limited search in this space a canonical set of parameters which allows us to describe generic behavior in a consistent way. Another important consideration in choosing the parameters relates to the numerical instabilities which were found to occur when the force coupling constant $g_{\sigma\bar\sigma}$, $g_{\sigma s}$, and g_{ss}, or the mean densities, were increased beyond certain threshold values. We found that these instabilities occur when the forcing terms cause the right-hand side of Eqs. (14) and (17) to become negative and are caused by a combination of the mean-field treatment of interparticle interactions and the restriction of the lattice-Boltzmann scheme to low Mach numbers. With these considerations in mind, and after a restricted search in the parameter space of the model we arrived at the following set of canonical parameters which, unless stated otherwise, are used throughout our simulations (the time step Δt is set to 1 throughout) $g_{\sigma\sigma}$ $=0$, $g_{\sigma\bar\sigma}=0.03$, $g_{\sigma s}=-0.01$, $g_{ss}-0.01$, $\tau_\sigma=\tau_s=1$, $\tau_d=2$, $m^\sigma=1$, $m^s=2$, $d_0=1$, and $\beta=10$. All calculations were performed on a 256^2 lattice subject to periodic boundary conditions. In the case of the binary oil-water systems we also performed additional calculations on 512^2 and 128^2 lattices in order to check for finite size effects.

The CPU time and memory requirements of our algorithm both scale $\sim L^D$, where L is the linear dimension of the lattice. In two dimensions we were able to study adequate system sizes using typical serial workstations. For example, simulation of a ternary system on a 256^2 lattice on a Silicon Graphics 250 MHz processor workstation takes just under 8 h to reach 3000 time steps (switching off the subroutines which perform the surfactant dynamics calculations reduces the CPU time by 50%.) For the present calculations we used a serial implementation of our lattice-Boltzmann algorithm. In three dimensions, however, the serial algorithm quickly becomes prohibitive in terms of computer memory for moderately sized systems. Fortunately, an important feature of LB is its intrinsically parallel structure and we have implemented a parallel version of our algorithm [18] which allows us to perform very large-scale 3D simulations on massively parallel platforms. We plan to report on the three-dimensional model in future publications.

A. Binary oil-water system

The dynamics of phase separation in a binary mixture, following a thermal quench into the unstable coexistence regime, proceeds by spinodal decomposition. Immediately after the quench, small domains, with local concentrations roughly corresponding to that of the two pure immiscible phases, spontaneously form and grow and finally result in complete phase separation [32]. To simulate phase separation we set up a simulation with equal quantities of water and oil with average densities 0.5, and no surfactant present (a ''critical quench''). This choice of average densities ensures that we are well within the immiscibility region of the model. The initial condition of these simulations is a uniform mixture of the two fluids with small random fluctuations in the uniform densities. These fluctuations are necessary to move the system out of a metastable uniform state, in which the mean-field forces are identically zero. The force term is initially set to zero and f_i^σ are set to $f_i^{\sigma(\mathrm{eq})}$ calculated from n^σ and $\tilde{\mathbf{u}}=0$ [Eq. (7)].

As can be seen from Fig. 1, immediately after the quench small domains spontaneously start to form. As time evolves, sharp interfaces develop between the regions associated with each phase, and the branchlike structures which were formed at the earlier stage of simulations coarsen. The growth of domains continues and, if left to run for a large enough time, the system would eventually reach the completely separated state of two distinct layers of fluid. Phase-separation experiments typically measure the structure factor $S(\mathbf{k},t)$, which contains information on the time evolution of the various length scales present in the system. It is defined as the Fourier transform of the density-density correlation function. For the discrete systems we are studying, we consider equivalently

$$S(\mathbf{k},t)=\frac{1}{N}\left|\sum_\mathbf{x}[q(\mathbf{x},t)-\bar{q}(t)]e^{i\mathbf{k}\cdot\mathbf{x}}\right|^2, \tag{29}$$

where $\mathbf{k}=(2\pi/L)(m\mathbf{i}+n\mathbf{j})$, $m,n=1,2,\ldots L$; here L is the linear lattice size, $N=L^2$ is the total number of grid points in the system, $q(\mathbf{x},t)=n^{\mathrm{water}}(\mathbf{x},t)-n^{\mathrm{oil}}(\mathbf{x},t)$ is the total color order parameter at grid point $\mathbf{x}$ and time t, and $\bar{q}(t)$ is the
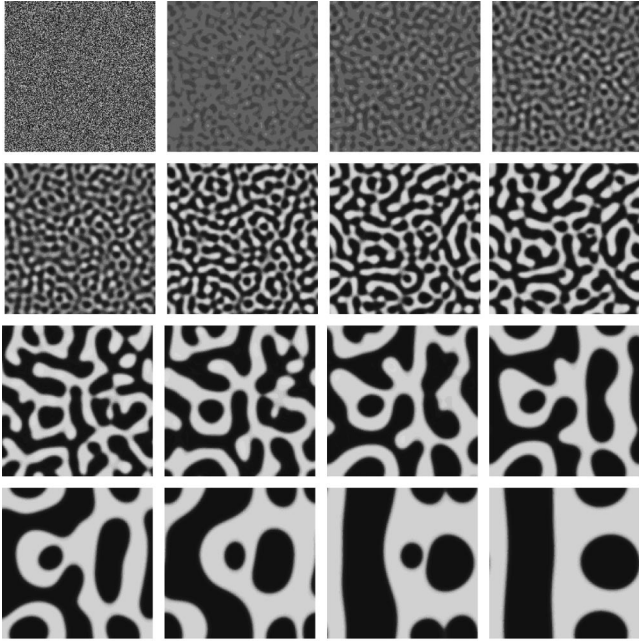
FIG. 1. Snapshots of phase separation of a binary oil-water mixture during a critical quench. From left to right and top to bottom time steps 0,800,1600,2400,3200,4800,6400,8000,12 000,16 000, 20 000,24 000,30 000,45 000,60 000,90 000 are shown. The system size is 256^2.

spatial average of q(**x**,t) at time t. $S(\mathbf{k},t)$ is further smoothed by averaging over an entire shell in **k** space to obtain the circularly averaged structure factor

$$S(k,t) = \frac{\sum_{\hat{k}} S(\mathbf{k},t)}{\sum_{\hat{k}} 1}, \qquad (30)$$

where the sum $\sum_{\hat{k}}$ is over a circular shell defined by $(n - \frac{1}{2}) \leq |\mathbf{k}|L/2\pi < (n + \frac{1}{2})$ and the cutoff wave vector k_c has the maximum possible value which is compatible with the periodicity in **k** space. We use the first moment of the circularly-averaged structure factor as a measure of the characteristic length scale of the system

$$k(t) = \frac{\sum_{k} kS(k,t)}{\sum_{k} S(k,t)}. \qquad (31)$$

The characteristic size of the domains is then given by $R(t) = 2\pi/k(t)$.

Figure 2 displays the temporal evolution of the circularly-averaged structure factor obtained for a critical quench in a 512^2 system. At early times in the simulations ($t < 4000$ time steps) we observed that the amplitude of the peak in the structure factor increases without the position of the peak changing in time. This behavior is indicative of initial sharpening of the domains, as the amplitude of the peak in $S(k,t)$ is proportional to the domain mass within a characteristic domain size. As time evolves further, the peak of $S(k,t)$
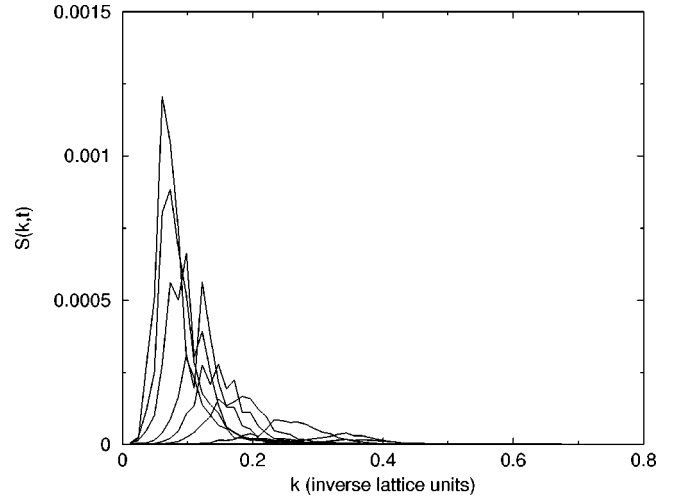

FIG. 2. Temporal evolution of $S(k,t)$ for a critical quench in a binary oil-water system. Time steps shown are, from bottom to top, $t = 3200,4000,6400,9600,12 000,14 400,20 000,24 000$. The system size is 512^2.

shifts to smaller wave numbers and its height increases, indicating the coarsening of the domains. At intermediate times we also observe the appearance of a second peak in $S(k,t)$, which later on becomes a shoulder of the main peak and then merges with it. After an initial transient regime, the dynamics of phase separation is often characterized by a single length scale. This length scale is usually described by a power law behavior $R(t) = t^{\alpha}$. Simple dimensional analysis of the hydrodynamical evolution equations in 2D yields for the domain growth exponent $\alpha = 2/3$, when the binary system is in the inertial hydrodynamic regime [32,33].

In Fig. 3 the time evolution of $R(t)$ is shown as obtained from our lattice-Boltzmann simulations with system size 512^2. Finite-size effects in this quantity are known to become important when $R(t)$ is comparable to the linear size of the lattice L. We checked these effects by performing addi-
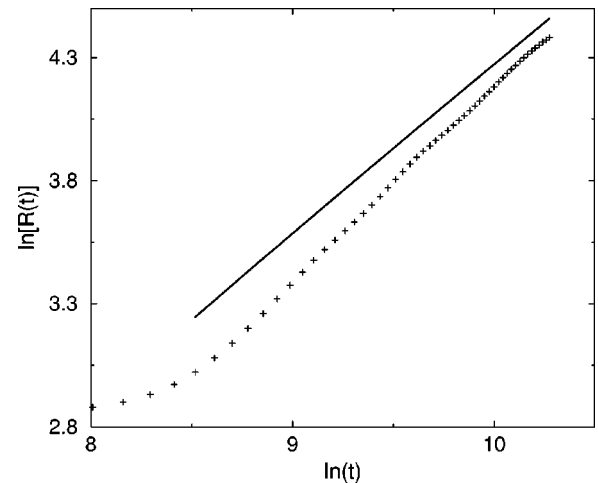

FIG. 3. Logarithm of the average domain size $R(t)$ (lattice units) as a function of the logarithm of the time (time steps) with data taken from lattice-Boltzmann simulations of a critical quench in binary immiscible phase separation. The straight line corresponds to a growth exponent $\alpha = 0.66$ and is provided as a guide to the eye only. The system size is 512^2.
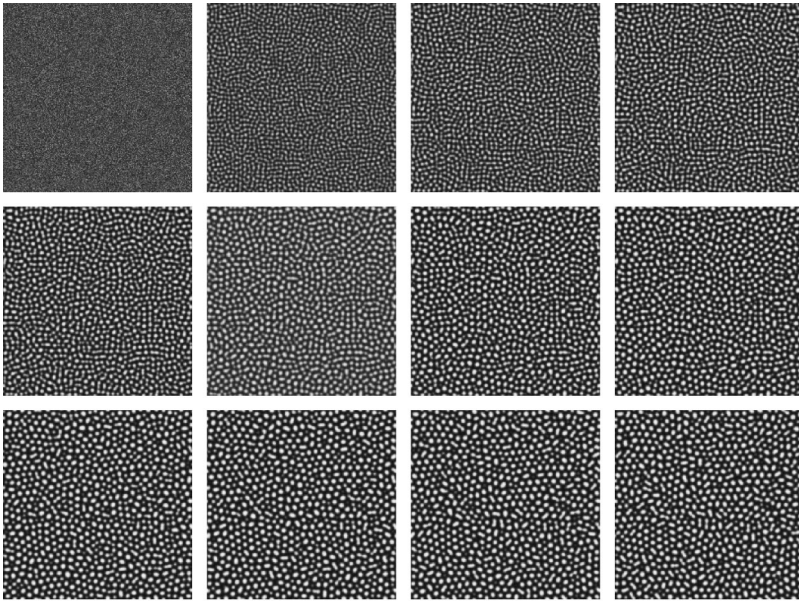
FIG. 4. Snapshots of time evolution of oil-in-water droplet microemulsion phase. From left to right and top to bottom time steps 0,200,400,600,800,1200,1600,2000,3000, 4000,5000,6000 are shown. The system size is 256^2.

tional calculations of $R(t)$ for system sizes 128^2 and 256^2. By comparing the results we deduced that finite-size errors in our 2D simulations become important when $R(t) \gtrsim L/5$. The 3D lattice-Boltzmann simulations of Kendon et al. [34] seem to indicate a somewhat larger value of $R(t)$ beyond which these errors become pronounced. This might indicate that finite-size effects are more significant in 2D. Discarding both the early-time transient regime and the late-time regime where finite-size effects are pronounced, we found that the late-time behavior of $R(t)$ in our simulations is $R(t) \sim t^{0.66 \pm 0.01}$, in good agreement with the abovementioned scaling arguments and previous lattice-gas [36] and lattice-Boltzmann [40] simulations of phase separation in 2D. We note, however, that this result is only a first qualitative study of the dynamics of phase separation within our model and more work is needed in order to unambiguously identify different scaling regimes within the parameter space of the model.

B. Microemulsion phases: oil droplets in water and sponge phase

We used our model to simulate the different ternary microemulsion phases that are possible in 2D, namely, the oil-in-water droplet and sponge phases. In experimental systems the two distinct microemulsion phases will form when the appropriate concentrations of oil, water, and surfactant are present in the system below the critical temperature. The oil-in-water droplet phase typically consists of finely divided spherical regions of oil, with stabilizing monolayers of surfactant surrounding them, embedded within a continuous water background. If one increases the relative amount of oil in the system and there is sufficient amphiphile present, one observes the formation of mutually percolating tubular regions of oil in water, with a monolayer of surfactant sitting at the interface. In both these cases, the equilibrium state does not correspond to complete separation of immiscible oil and water regions, but rather to complex structures with very different characteristic length scales that form as the result of the presence of amphiphile [10].

In order to reproduce the oil-in-water droplet phase, we set up a simulation with a uniform mixture of oil, water, and surfactant with small density fluctuations as our initial configuration. The average densities of oil, water, and surfactant are 0.42, 0.6, and 0.1, respectively. Figure 4 displays the results. We see the rapid formation of many small oil-in-water droplets, whose size initially increases slightly, but not without limit. This is characteristic of the experimental droplet phase. It occurs because the free energy penalty associated with the existence of many oil-water interfaces in this phase, as compared to the complete oil-water phase separation, is compensated by the gain in free energy due to adsorption of surfactant dipoles at these interfaces. If coarsening of oil droplets was to continue the interface area for adsorption of surfactant dipoles would decrease resulting in an increase in the amount of surfactant in bulk water or oil. The free energy penalty for bulk surfactant prevents this from happening. The concentration of the surfactant is not visible in Fig. 4, but is high at the interface and low in oil-rich and water-rich regions, with the surfactant dipoles at the interface pointing on average from water-rich region towards the oil-reach droplets (see also Fig. 1 and Fig. 2 in Ref. [25]).

In order to further quantify the result we show in Fig. 5 the time evolution of the circularly averaged structure factor $S(k,t)$. Once again we observe the formation of a distinct peak in the structure factor, indicating the sharpening of the domains. Interestingly, this happens much faster than in the case of the binary system. The presence of the surfactant seems to accelerate domain formation in the early stage of phase separation, an effect which has also been seen in the hybrid Ginzburg-Landau simulations of Kawakatsu et al. [35], and should be detectable experimentally. As time evolves the peak in $S(k,t)$ increases in height and shifts further towards smaller values of the wavelength, indicating the growth of droplets. From at least time step 5000 onwards there appears to be a negligible amount of further movement of the position of the peak, indicating that droplets have reached a maximum size and will grow no more. We observed small oscillations in the intensity of the peak in
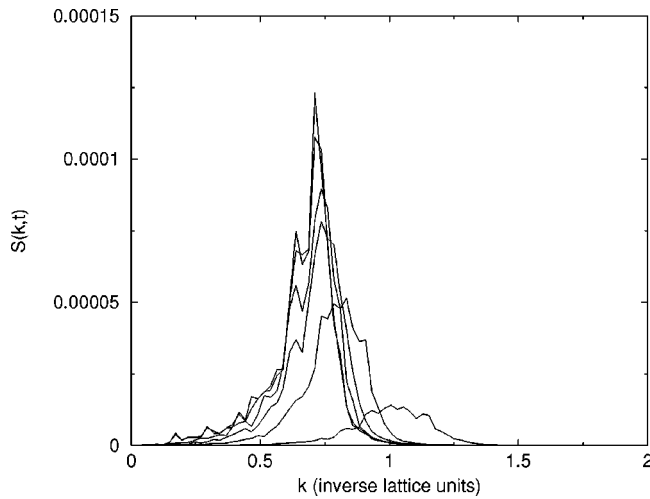
FIG. 5. Temporal evolution of the circularly-averaged structure factor $S(k,t)$ for the microemulsion droplet phase shown in Fig. 4. Time steps shown, from bottom to top, are $t=200,1000,2000,3000,5000,6000$.
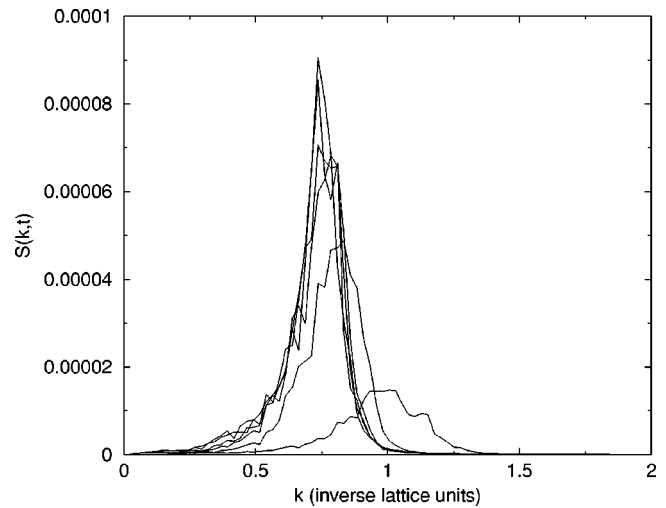

FIG. 7. Temporal evolution of the circularly-averaged structure factor $S(k,t)$ for the sponge microemulsion phase shown in Fig. 6. Time steps shown, from bottom to top, are $t=200,1000,2000,3000,4000,6000$.

$S(k,t)$ which suggest that the characteristic domain mass fluctuates in time.

To investigate the ability of the model to access the sponge phase, we set the average densities of water and oil both equal to 0.5 while keeping the average density of surfactant at the same value as before. The results are shown in Fig. 6. Starting once again from a perturbed uniform mixture of fluids, this time we observe the growth of an interconnected network of tubular regions of oil and water. The width of the oil and water regions grows in size up to about 4000 time steps. During this time the surfactant particles, which were initially distributed uniformly in the system, concentrate around the various oil-water interfaces. Beyond this stage the system changes very little, indicating that the observed sponge phase is stable. This is also confirmed by our result for the circularly-averaged structure factor shown in Fig. 7.

C. The effect of surfactant on domain growth dynamics

To further investigate the effect of surfactant on domain growth dynamics in the sponge-phase we performed additional simulations in which we kept the average density of oil and water fixed at 0.5 while gradually increasing the amount of surfactant in the system. The average densities of surfactant used in these simulations are 0.05,0.1,0.15, 0.20,0.30. We analyze the effect of varying the surfactant concentration using the domain size $R(t)$ as a quantitative measure. The domain size is calculated from the circularly averaged structure factor, as described in Sec. II. The results are summarized in Fig. 8 where the domain sizes are plotted against time, and as a function of increasing surfactant concentration. The presence of the surfactant significantly retards the growth of the domains and it can be clearly seen that for surfactant concentrations larger than 0.05, the domain size reaches saturation. Following Boghosian, Cov-
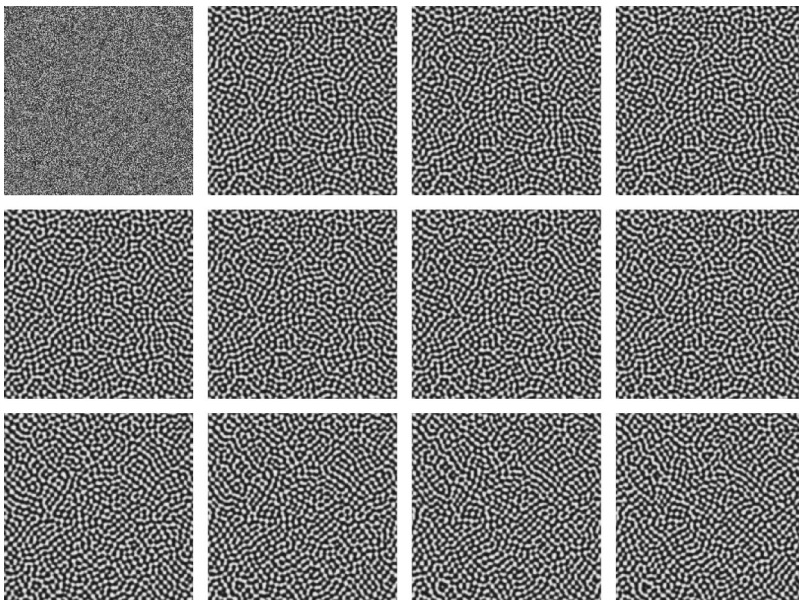

FIG. 6. Snapshots of time evolution of sponge microemulsion phase. From left to right and top to bottom time steps 0,200,400,600,800,1200, 1600,2000,3000,4000,5000,6000 are shown. The system size is 256^2.
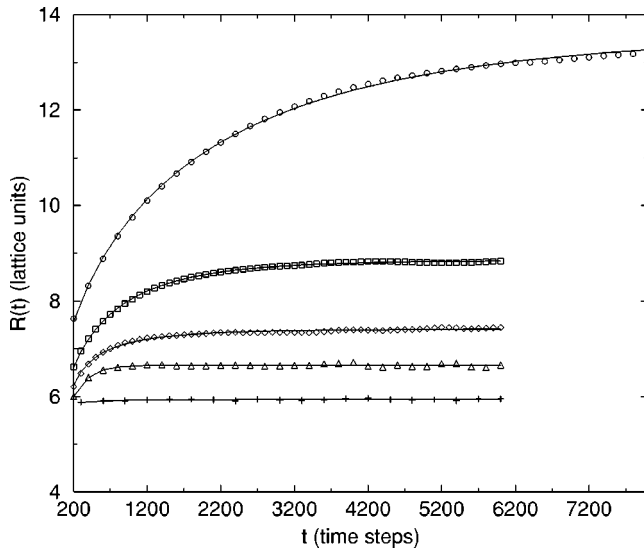
FIG. 8. Time evolution of average domain size $R(t)$ (lattice units) in a ternary system with equal concentrations of water and oil (0.5). Curves from top to bottom correspond to systems with average surfactant concentration 0.05,0.1,0.15,0.2,0.3. The full lines are the stretched exponential fits to our data.

eney, and Emerton [36], we analyzed the time-dependence of domain growth in terms of a stretched exponential form

$$R(t) = R_\infty - a \exp(-ct^d), \tag{32}$$

where R_∞, a, c, and d are adjustable parameters, which are determined by a least-square fit to our data. As can be seen from Fig. 8 this form fits our results extremely well across the full time scale of the simulations and for all surfactant concentrations considered. We also investigated a fit of the logarithmic form $R(t) = a + b(\ln t)^c$, which describes the phase-separation of binary alloys in the presence of impurities [37]. Obviously, this form is unable to describe the late time saturation of the domain size and we found that the root-mean-square errors using this form to describe the early times of domain formation are also an order of magnitude larger than those of the stretched exponential form. In the case with average surfactant density equal to 0.05 the domain size does not saturate; nevertheless Eq. (32) provides a better fit to the slow growth of the domain size than the logarithmic form for the time interval we considered ($0 < t \leqslant 12\,000$). LGA simulations [36,38] indicate, however, that the logarithmic from is a good fit for describing the dynamics of ''metastable'' (i.e., long-lived) emulsions which do eventually phase separate.

At late times in these simulations, small but persistent oscillations in $R(t)$ can be seen in Fig. 8, which are absent in the case of binary systems. These oscillations have also been observed in LGA simulations, both in 2D [36] and in 3D [38]. Their presence in our lattice-Boltzmann simulations confirms that these oscillations are caused by the additional dynamics which the presence of amphiphile introduces into the system: they are not a consequence of statistical fluctuations inherent in LGA.

Finally, we investigate the relationship between the final size of the domains and the surfactant concentration. Laradji *et al.* [41] used simplified MD simulations to study the dy-
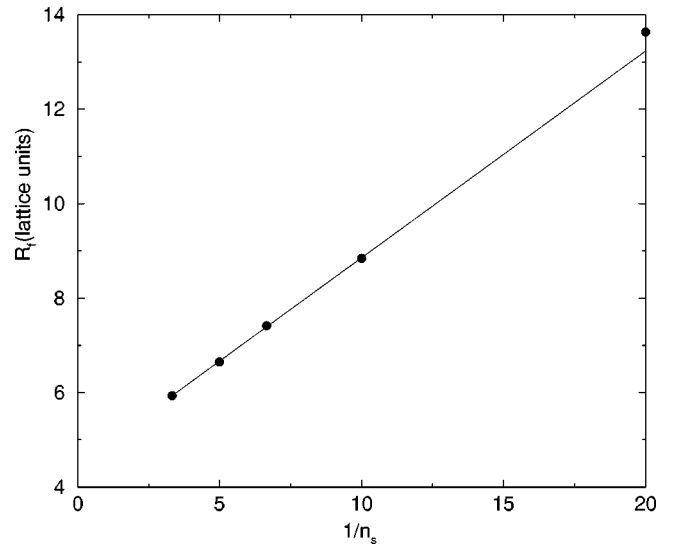

FIG. 9. Final domain sizes R_f (lattice units) as a function of the inverse of the surfactant concentration $1/\bar{n}_s$. The solid line is a linear fit to the first four points of our data.

namics of ternary oil-water-surfactant systems and found that the final domain size R_f is inversely proportional to the average concentration of surfactant molecules $\bar{n}_s$:

$$R_f \sim \frac{1}{\bar{n}_s}. \tag{33}$$

In the deep quenches performed by Laradji *et al.* surfactant molecules entirely reside at the interfaces. This was not the case in the lattice-gas simulations of Emerton *et al.* [36] in which a certain amount of surfactant existed as monomer in bulk oil or water. After subtracting away from $\bar{n}_s$ a background monomer density, these authors also found a linear relationship between R_f and $1/\bar{n}_s$. A similar situation to lattice-gas simulations occurs in our simulations where a significant fraction of surfactant exists as monomers in bulk oil or water. However, we found that even without correcting for the background monomer density of surfactant Eq. (33) gives a very good description of the relationship between R_f and $\bar{n}_s$. This is shown in Fig. 9 where R_f is plotted versus the inverse of $\bar{n}_s$. The condition that all surfactant molecules should be at the interface does not therefore seem necessary for Eq. (33) to hold, as long as the surfactant molecules are mainly concentrated at the interface.

D. Ternary phase: Lamellae

Next we use our model to investigate the stability of a lamellar structure, which is composed of alternating layers of oil-rich and water-rich phases separated by a layer of surfactant. A preliminary discussion was given in [25]. We look at the system with and without surfactant present in order for a critical comparison to be made. A similar investigation of the lamellar structure in 2D and in 3D has been performed previously using LGA [26,39]. In a similar way to those simulations, we set up the initial configuration of the system as
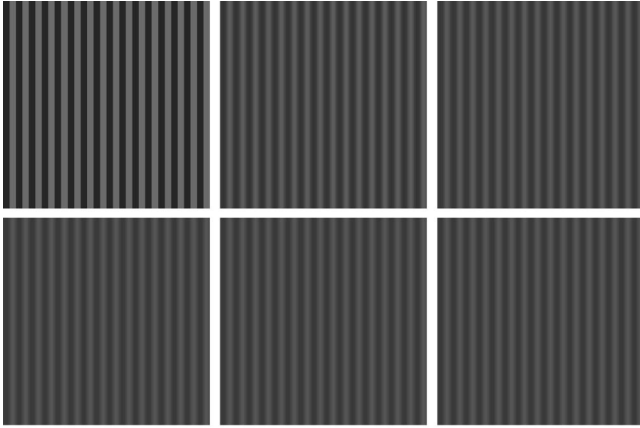
FIG. 10. Snapshots of the evolution of the lamellar structure in the absence of surfactant. Time steps shown are clockwise from top to bottom $t = 0,300,600,3000,6000,9000$. The system size is 256^2.

layers of pure oil and pure water eight sites wide such that each species has an average density 1.0.

Snapshots of our simulations for the binary case are shown in Fig. 10 for time steps $t \leq 9000$. As can be seen from this figure, the initial layered structure becomes less sharply defined as time evolves but the lamellar structure remains intact and does not evolve to complete phase separation. By letting the simulations run for much longer times (30 000 time steps), we checked that the lamellar structure is indeed the final equilibrium state of the system and we are not observing a metastable state with long equilibration time. We also examined the stability of the structure against small fluctuations in the density and found the lamellar structure to remain stable. These results are in sharp contrast with the previous LGA simulations in which, starting from a layered structure, complete phase separation was observed [26]. As pointed out in Ref. [25], in an infinite two-dimensional system with finite-temperature fluctuations, one expects lamellar structures to be unstable, due to Peierls instabilities [42]. The Peierls theorem, however, does not make any statement about the stability of such structures in finite 2D systems. The stability of the lamellar structure seen in our lattice-Boltzmann simulations and its instability in LGA simulations thus provides numerical evidence that the Peierls mechanism is also capable of destabilizing periodic layered structures in finite systems.

Next we examine the effect of surfactant on the layered structure by setting up a simulation where there is, in addition to water and oil layers, a single layer of surfactant at each of the oil-water interfaces. The average density of surfactant in each monolayer was 1.0 and the initial condition for the surfactant dipole vectors at each site was $\mathbf{d}(\mathbf{x},0) = 0$. We found that the final state of the system is, once again, lamellar. The presence of surfactant, however, causes the water-oil interfaces to remain sharper than in the previous simulations. This effect is shown in Fig. 11 (top panel) where the initial and final state of the color order parameter (averaged over the y direction, the direction perpendicular to layers) are plotted along the x axis for both sets of simulations.

Due to the symmetry of the system d_y, the component of the dipole vector in the y direction, does not evolve in time from the initial condition $d_y = 0$. Under, the influence of the
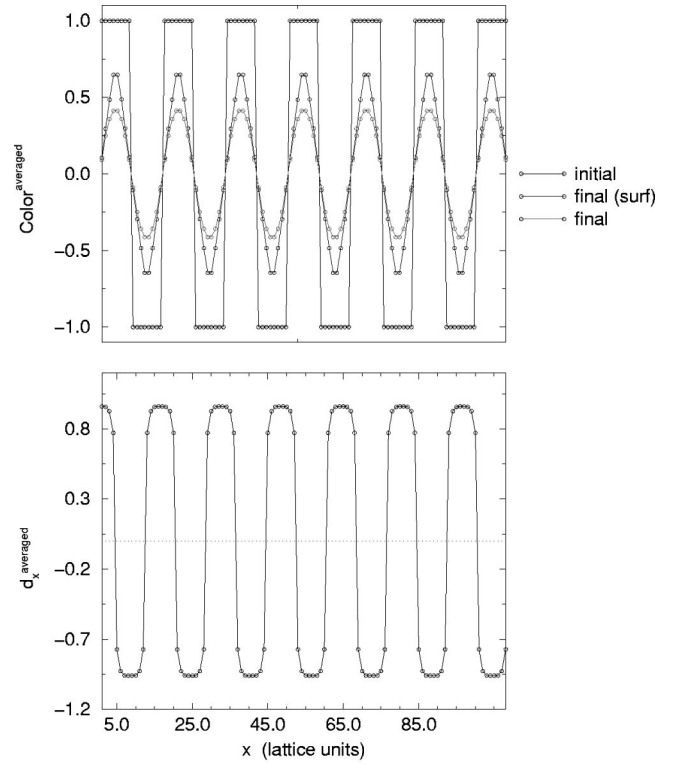

FIG. 11. Upper panel shows the final state color order parameter, averaged over the y direction (vertical in Fig. 10) of lamellar structure, both with and without surfactant present. The time step shown is 9000. Note how the presence of surfactant sharpens the interfaces between water and oil. Lower panel shows the final state distribution of the surfactant directors (in lattice units), averaged over the y direction at time step 9000. The system size is 256^2.

field set up by the color gradient, however, d_x does evolve in time. A plot of the final state of d_x, averaged in the y direction, is shown in Fig. 11 (lower panel). It can be seen that the surfactant directors have their largest values around the interfaces, i.e., at the points where the color order parameter changes sign. It is interesting, albeit expected, that the surfactant dipoles alter alignment, always pointing from water-rich to oil-rich layers. The reason for this behavior is that, neglecting surfactant-surfactant interactions, the direction of the equilibrium dipole vectors in our model is determined by the gradient of the color order parameter, as can be seen by expanding Eq. (24) in a Taylor series in the ratio of $|\mathbf{c}_i|$ to the color gradient scale length. For the lamellar structure, the color order parameter changes only in the x direction with its slope changing sign alternately, in passing from a water-rich layer to an oil-rich layer; as can be seen in Fig. 11 the surfactant dipole vectors flip direction every time this happens.

E. Self-assembly in mixtures of water and surfactant

Repeating the simulations performed for the ternary mixtures but setting the average density of oil (or water) to zero gives results for binary water and surfactant systems. We kept the average density of water fixed at 0.5 and performed two simulations, one with a high surfactant density $\bar{n}_s = 0.25$ and one with a low surfactant density $\bar{n}_s = 0.071$. Snapshots of the simulation for the case of high surfactant concentration are shown in Fig. 12. It can be seen that start-
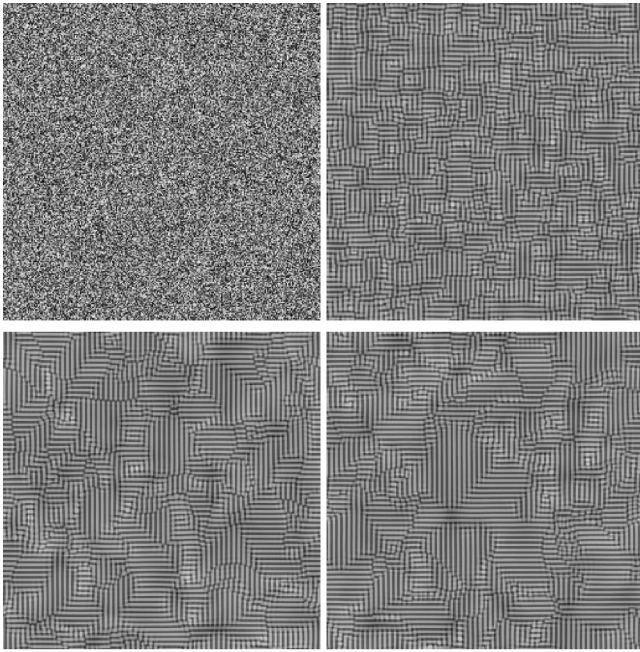
FIG. 12. Snapshots of self-assembly of a uniform mixture of water and surfactant into lamellar domains. From left to right and top to bottom time steps 0,300,3000,9000 are shown. The surfactant-water density difference is shown in gray scaling with black corresponding to high surfactant density and white corresponding to high water density. The average concentrations of water and surfactant are 0.5 and 0.25, respectively. The system size is 256^2.

FIG. 13. Upper panel shows variation of the water density within an ''anti-ferromagnetic'' domain averaged over the y direction (which is vertical in Fig. 12) within the domain. The middle panel shows variation of surfactant density within the same domain. The lower panel shows the final state distribution of the d_x (circles) and d_y (squares) of surfactant directors, averaged over the y direction (in lattice units). The time step shown in all panels is 3000.

ing from a uniform mixture of water and surfactant, the system organizes itself in small domains each of which has a clear lamellar structure consisting of alternating water-rich and surfactant-rich layers. These domains grow in time but not without limit. They are highly dynamic objects which continuously form and disintegrate but whose average size does not grow in time once they are formed. In Fig. 13 we display the variation of water and surfactant densities within one of the domains, as an example. The densities are averaged over the y direction within the domain and are displayed along the x axis (the direction of density modulations within this domain). Also shown are d_x and d_y components of surfactant directors. It can be seen that the domain is built up of a stack of surfactant-rich bilayers separated by water-rich layers each ~ 2 lattice units wide. The surfactant directors are ordered antiferromagnetically within each domain, such that only the hydrophilic heads of surfactant molecules are exposed to water-rich regions. In the case of the system with low surfactant density visualization of the data indicates the existence of weak density modulations in the system but without any clear domain formation.

To further quantify the dynamics of self-assembly in the binary water-surfactant system we make use of the circularly-averaged surfactant structure factor. In Fig. 13 we show $S(k,t)$ at time steps 0, 1000, and 2500 for both systems. It can be seen that in both cases $S(k,t)$ has a peak around $k = 1.6$. This peak corresponds to the repeat period of water and surfactant density modulations and its position becomes stable already for $t < 100$ time steps. In the case of the system with high surfactant concentration we see the emergence of a second peak in $S(k,t)$ at much smaller wavevectors,
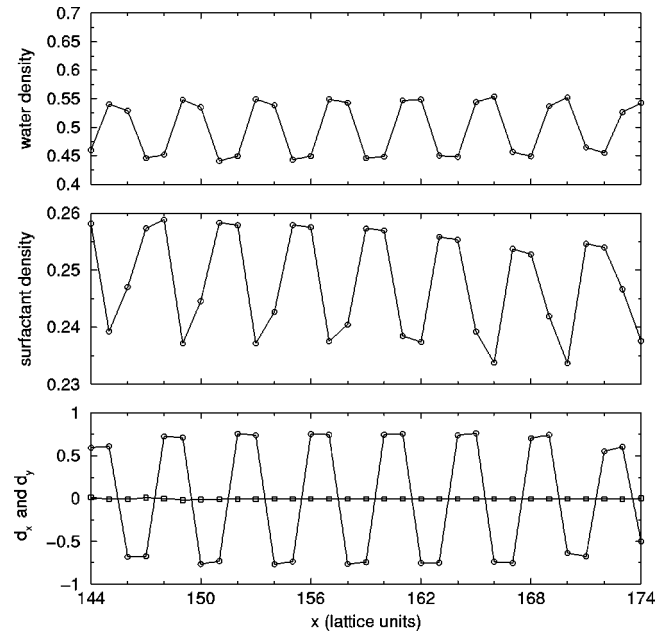
indicating that there is another characteristic length scale in this system, namely, the average size of lamellar domains.

In order to identify the driving force behind self-organization of the system we performed two additional calculations, using the same initial conditions as before. One simulation was performed with dipolar interactions among surfactant molecules switched off ($g_{ss} = 0$) while in the other simulation we kept $g_{ss} - 0.01$ but switched off the coupling between surfactant and water molecules, by setting $g_{\sigma s}$ to 0. In Figs. 14 and 15 the spherically averaged structure factor is shown at time step 2500 as obtained from these simulations. For comparison $S(k,t)$ of the full simulations is also shown at the same time step. It can be seen that switching off the interaction between surfactant dipoles results in a structure factor which has only a single peak near $k = 1.6$ while switching off water-surfactant interaction results in a structure factor with only a peak near $k = 0$. This provides clear evidence that water-surfactant interactions are responsible for the formation of alternating water-rich and surfactant-rich layers while formation of domains is a consequence of dipolar interactions between surfactant particles.

IV. CONCLUSIONS

Building on our recent work [25] we developed in this paper a lattice-Boltzmann model for ternary interacting amphiphilic fluids. The main features of the model are that interactions among fluid components are realized by introducing self-consistently generated mean-field forces between different species and that the orientational degrees of freedom of amphiphilic species are explicitly modeled. The mean-field force is incorporated into the scheme in a way which is consistent with the kinetic theory of interacting flu-
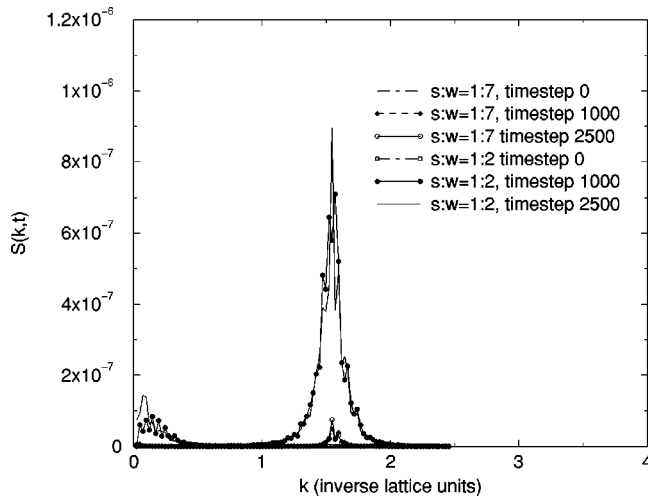
FIG. 14. Circularly-averaged surfactant density structure factor $S(k,t)$ for binary water and surfactant mixtures shown at time steps 0 and 2500 for a 256^2 binary water-surfactant system. The average density of water is kept at 0.5 while the surfactant average density is increased from 0.071 ($s:w=1:7$) to 0.25 ($s:w=1:2$). For both systems $S(k,t)$ has a peak near $k=1.6$ whose position corresponds to the repeat period of the lamellae. The peak near $k=0$ is present only for the system with high surfactant concentration and it signals the formation of lamellar domains whose average size correspond to the position of this peak.
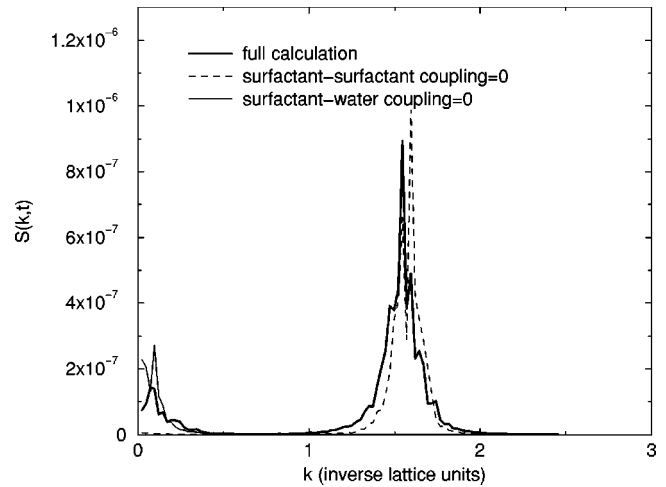

FIG. 15. Circularly-averaged surfactant density structure factor $S(k,t)$ for a binary water and surfactant mixture at time step 2500 calculated with both water-surfactant and surfactant-surfactant coupling swtiched on (thick solid line), only surfactant-water coupling switched on (dashed line) and only surfactant-surfactant coupling switched on (thin solid line). The system size is 256^2. The average concentrations of water and surfactant are 0.5 and 0.25, respectively.

ids mixtures and we provided a physical interpretation for the action of this force in terms of off-diagonal matrix elements in the BGK collision operator.

Using a single set of force coupling constants, we have shown that our model exhibits the correct 2D phenomenology for both binary and ternary phase systems. Various experimentally observed self-assembling structures form in a consistent way as a result of altering the relative amounts of oil, water and amphiphile in the system. The presence of enough surfactant clearly arrests the growth of the domains and we showed that when this happens the final domain size is inversely proportional to the amount of surfactant present in the system, in agreement with previous molecular dynamics simulations. Our study of the stability of the lamellar structure in 2D confirmed a striking difference between lattice-gas and lattice-Boltzmann simulations which result from the absence of fluctuations in the lattice-Boltzmann scheme [25]. Self-assembly into a local lamellar structure, as found in our simulations, has not been reported previously for binary water-surfactant systems but has been observed in microemulsion experiments performed on ternary water, oil and surfactant systems [43]. Our additional calculations indicate that by increasing the force coupling constants beyond a certain value the global lamellar phase, which has been reported previously [10,44], can also be reached in our model. The ability of our model to simulate self-assembly of

surfactant aggregates in a binary water-surfactant system clearly distinguishes our model from other existing lattice-Boltzmann schemes [13–15] which do not incorporate the vectorial nature of surfactant molecules and are therefore unable to describe the formation of such aggregates.

Natural refinements of our model would be the inclusion of fluctuations, e.g, via a fluctuating force term compatible with the fluctuation-dissipation theorem [45] which enables the system to move out of its metastable states. Also, some of the instabilities which we encountered in the present model might be mitigated by using more realistic forms for the interaction between different molecules and by adding the Enskog corrections for the collisions in dense systems [23] to the BGK collision operator. Our recently developed parallel [18] version of the lattice-Boltzmann model should allow us to extend the present study to 3D for which much more experimental data is available. This will help us to select parameters so that the model will provide a more realistic description of experimental observations; we also hope to then study various important phenomena such as flow of complex fluids in porous media.

[1] For a recent review see S. Chen and G. D. Doolen, Annu. Rev. Fluid Mech. **30**, 329 (1998).

[2] F. Higuera, S. Succi, and R. Benzi, Europhys. Lett. **9**, 345 (1989).

[3] G. McNamara and G. Zanetti, Phys. Rev. Lett. **61**, 2332 (1988).

[4] F. J. Higuera and J. Jemenéz, Europhys. Lett. **9**, 663 (1989).

[5] S. Y. Chen, H. D. Chen, D. Martinéz, and W. Matthaeus, Phys.

Rev. Lett. **67**, 3776 (1991).

[6] D. H. Rothman and J. M. Keller, J. Stat. Phys. **52**, 1119 (1988); A. K. Gunstensen, D. H. Rothman, S. Zaleski, and G. Zanetti, Rev. Mod. Phys. **43**, 4320 (1991).

[7] X. Y. He and L.S. Luo, Phys. Rev. E **55**, R6333 (1997).

[8] X. Shan and X. Y. He, Phys. Rev. Lett. **80**, 65 (1998).

[9] W.M. Gelbart, D. Roux, and A. Ben-Shaul, *Modern Ideas and Problems in Amphiphilic Science* (Springer, Berlin, 1993).

[10] G. Gompper and M. Schick, Phase Trans. Crit. Phenom. **16**, 1 (1994).

[11] J-B. Maillet, V. Lachet, and P. V. Coveney, Phys. Chem. Chem. Phys. **1**, 5277 (1999).

[12] J. S. Rowlinson and B. Widom, *Molecular Theory of Capillarity* (Clarendon Press, Oxford, 1982).

[13] A. Lamura, G. Gonnella, and J.M. Yeomans, Europhys. Lett. **45**, 314 (1999).

[14] O. Theissen, G. Gompper, and D. M. Kroll, Europhys. Lett. **42**, 419 (1998).

[15] O. Theissen and G. Gompper, Eur. Phys. J. B **11**, 91 (1999).

[16] M. Swift, W. Osborn, and J. Yeomans, Phys. Rev. Lett. **75**, 830 (1995); M. Swift, S. Orlandini, W. Osborn, and J. Yeomans, Phys. Rev. E **54**, 5041 (1996).

[17] X. Shan and H. Chen, Phys. Rev. E **47**, 1815 (1993); X. Shan and H. Chen, *ibid.* **49**, 2941 (1994).

[18] M. Nekovee, J. Chin, and P. V. Coveney, *Simulation '99* 11, edited by J. K. Pollard and D. Al-Dabas (London, 1999).

[19] P. Bhatnagar, E. Gross, and M. Krook, Phys. Rev. **94**, 511 (1954).

[20] S. Chen, H. Chen, D. Martinez, and W. Matthaeus, Phys. Rev. Lett. **67**, 3776 (1991); H. Chen, S. Chen, and W. Matthaeus, Phys. Rev. A **45**, 5339 (1992).

[21] Y. Qian, D. d'Humières, and P. Lallemand, Europhys. Lett. **17**, 479 (1992).

[22] J. A. Schouten, Phys. Rep. **172**, 33 (1989).

[23] See, for example, J. H. Ferziger and H. G. Kaper, *Mathematical Theory of Transport Process in Gases* (North-Holland, Amsterdam, 1972).

[24] X. Y. He, X. Shan, and G.D. Doolen, Phys. Rev. E **57**, R13 (1998).

[25] H. Chen, B. M. Boghosian, P. V. Coveney, and M. Nekovee, Proc. R. Soc. London, Ser. A **456**, 2043 (2000).

[26] B. M. Boghosian, P. V. Coveney, and A. N. Emerton, Proc. R. Soc. London, Ser. A. **452**, 1221 (1996).

[27] S. Bastea and J. L. Lebowitz, Phys. Rev. Lett. **78**, 3499 (1997).

[28] L. S. Luo, Phys. Rev. Lett. **81**, 1618 (1998).

[29] N. Martys, X. Shan, and H. Chen, Phys. Rev. E **58**, 6855 (1998).

[30] See for example, N. H. March, and M. Parinello, *Collective Effects in Solids and Liquids* (Adam Hilger, New York, 1982).

[31] G. Arfken, *Mathematical Methods for Physicists* (Academic Press, London, 1985).

[32] A. J. Bray, Adv. Phys. **43**, 357 (1994).

[33] H. Furakawa, Physica A **123**, 497 (1984).

[34] V. M. Kendon, J-C. Desplat, P. Bladon, and M.E. Cates, Phys. Rev. Lett. **83**, 576 (1999).

[35] T. Kawakatsu, K. Kawasaki, M. Furusaka, and T. Kanayo, J. Chem. Phys. **99**, 8200 (1993).

[36] A. N. Emerton, P.V. Coveney, and B. M. Boghosian, Phys. Rev. E **55**, 708 (1997).

[37] M. F. Gyure, S. T. Harrington, R. Strilka, and H. E. Stanley, Phys. Rev. E **52**, 4632 (1995).

[38] P. Love, P. V. Coveney, and B. M. Boghosian (unpublished).

[39] B. M. Boghosian, P. V. Coveney, and P. Love, Proc. R. Soc. London, Ser. A **456**, 1431 (2000).

[40] F. J. Alexander, S. Chen, and D. W. Grunau, Phys. Rev. B **48**, R634 (1993).

[41] M. Laradji, O. G. Mouritsen, S. Toxvaerd, and M. J. Zuckermann, Phys. Rev. E **50**, 1243 (1994).

[42] R. E. Peierls, *Quantum Theory of Solids* (Clarendon Press, Oxford, 1955).

[43] C. G. Vonk, J. F. Billman, and E. Kaler, J. Chem. Phys. **88**, 3970 (1988).

[44] M. W. Matsen and D.E. Sullivan, Phys. Rev. A **41**, 2021 (1990).

[45] A. J. C. Ladd, Phys. Rev. Lett. **70**, 1339 (1993); A. J. C. Ladd, J. Fluid Mech. **271**, 285 (1994).